THE TEMPERATURE DISTRIBUTION IN A FULL-SCALE STEEL FRAMED BUILING SUBJECT TO A NATURAL FIRE

* František Wald[1)], Magdalena Chladná[2)], David Moore[3)], Aldina Santiago[4)] and Tom Lennon[5)]

[1)]Czech Technical University in Prague, Czech Republic
[2)]Technical University, Bratislava, Slovak Republic
[3)] British Constructional Steelwork Association, London, United Kingdom
Building Research Establishment, Garston, United Kingdom
[4)]University of Coimbra, Portugal
[5)]Building Research Establishment, Garston, United Kingdom
[1)]wald@fsv.cvut.cz

ABSTRACT

Current fire design codes for determining the temperature within the structural elements that form part of a complete building are based on isolated member tests subjected to the standard fire. However, the standard time-temperature response bears little relation to real fires and does not include the effects of differing ventilation conditions or the influence of the thermal properties of compartment linings. The degree to which temperature uniformity is present in real compartments is not addressed and direct flame impingement may also have an influence, which is not considered. It is clear that the complex thermal environmental that occurs within a real building subject to a natural fire can only be addressed using realistic full-scale tests.

To study global structural and thermal behaviour, a research project was conducted on the eight storey steel frame building at the Building Research Establishment's Cardington laboratory. The fire compartment was 11 m long by 7 m wide. A fire load of 40 kg/m^2 was applied together with a dead load of 3,65 (??) kN/m^2 and an imposed load of 3,50 kN/m^2. This paper summarises the experimental programme and presents the time-temperature development in the fire compartment and in the main supporting structural elements. Comparisons are also made between the test results and the temperatures predicted by the structural fire Eurocodes.

[1)] Professor
[2)] Lecturer
[3)] Director check David's new job title
[4)] Lecturer

[5)] Senior researcher

INTRODUCTION

It has long been recognised that global frame behaviour differs from an assessment based upon the performance of the individual elements, which go to make up a structure. The experience gained from investigations following the catastrophic gas explosion at Ronan Point which led to a progressive structural collapse highlighted the need for the engineer to consider global behaviour which, in this instance, led to a failure mechanism not considered at the design stage. Subsequent robustness requirements have led to improvements in the design and construction of framed structures. Just as a consideration of overall building behaviour can lead to previously unconsidered modes of collapse so such a philosophy may reveal beneficial aspects of frame behaviour. As well as potential disasters to be avoided there may be potential advantages to be utilised. Alternative methods of sustaining the applied loading may be available. Attempts to demonstrate the enhanced performance available through frame continuity were made as far back as the 1930's (Steel Structures Research Committee). Moore et al (Moore, 1993) provided a comprehensive justification for testing at full scale. The principles of assessing the structural performance of individual members when subject to realistic loading regimes and realistic boundary conditions are particularly relevant when considering the fire resistance of a framed structure.

The development of the Large Building Test Facility at the Building Research Establishment's (BRE) Cardington laboratory near Bedford in the UK provided the construction industry with a unique opportunity to carry out full-scale fire tests on a complete steel framed building designed and built to UK practice but in such a way that it satisfied the requirements of Eurocode 3. Consequently between the 1995 and early 2003 a series of seven large scale fire tests were conducted on a full-scale steel framed building at Cardington. This paper describes the last of these fire tests and presents the measured temperatures within the compartment, through the main supporting steel and composite floor and the temperature distribution in each of the main beam-to-column and beam-to-beam connections

The Test Facility

To meet the needs for the future the BRE created the Large Building Test Facility within one of the airship hangar's at Cardington, south of Bedford in the UK. The hangar is approximately 260 m long, 80 m wide and 50 m high and contains a 70 m by 50 m strong floor at one end. This facility can accommodate full-sized buildings up to ten storeys high within a weatherproof envelope.

The opportunities for testing and assessment of methodologies, techniques and materials for buildings and structures erected in the facility are limited only by the closed environment and the unique foundation and as always by the imagination of those undertaking the work. Physical tests involving static loads, dynamic vibrations, fire, explosion, heat and water can all be used in simulations of a wide range of realistic hazard scenarios.

The facility currently contains three large experimental buildings (Moore, 1995). These are a six storey timber structure, a seven storey concrete structure and an eight storey steel building.

The Test Structure

The first structure to be erected within the LBTF was an eight-storey steel framed building. This building was designed and constructed to resemble a typical modern city-centre, eight-storey office block. The building covers an area of 21 m by 45 m, with an overall height of 33 m. It consists of five 9 m bays along the length of the building and across the width there are

three bays spaced at 6 m, 9 m and 6 m. The building has three lift-shafts, one in the centre of the building and two placed at each end. The structure was designed as a braced frame with lateral restraint provided by cross-bracing around the three vertical access shafts. The beams were designed as simply supported acting compositely (via shear studs) with the lightweight composite floor slab. The floor slab is 130 mm deep and consists of a steel trapezoidal deck with lightweight concrete and an A146 steel anti-crack mesh.

The connections were designed and detailed to the BCSA/SCI 'greenbook', Joints in Simple Construction. Fin plates were chosen for most of the beam-to-beam connections. In most cases, this meant that the secondary beams were simply sawn, drilled and notched. Flexible end-plates were adopted for the main beam-to-column connections. These provided a little more rigidity to the steel frame during erection.

Throughout the structural design the underlying philosophy was to obtain a structure that was buildable and at all stages of construction and erection reflected normal building practice in the UK rather than specialist research procedures.

The building was designed for a load of 2,5 kN/m^2 imposed plus 1,0 kN/m^2 for partitions on all floors except the roof which was designed for a plant loading of 7,5 kN/m^2.

THE FIRE TEST

The structural integrity fire test (large test No.7) was carried out in a centrally located compartment of the building, enclosing a plan area of 11 m by 7 m on the 4th floor (Wald et al, 2003). The preparatory works took four months. The fire compartment was bounded with walls made of three layers of plasterboard (15 mm + 12,5 mm + 15 mm) with a thermal conductivity of between 0,19 - 0,24 Wm^{-1}K^{-1}. In the external wall the plasterboard is fixed to a 0,9 m high brick wall. The opening of 1,27 m high and 9 m length simulated an open window to ventilate the compartment and allow for observation of the element behaviour. The ventilation condition was chosen to produce a fire of the required severity in terms of maximum temperature and overall duration. The columns, external joints and connected beam (about 1,0 m from the joints) were fire protected to prevent global structural instability. The fire protection used was 18 - 22 mm of Cafco300 vermiculite-cement spray, with a thermal conductivity of 0,078 Wm^{-1}K^{-1}.

The steel exposed structure consists of two secondary beams (section 305x165x40UB, steel S275 measured f_y = 303 MPa; f_u = 469 MPa), an edge beam (section 356x171x51UB), two primary beams (section 356x171x51UB, steel S350 measured f_y = 396 MPa; f_u = 544 MPa) and four columns, (internal column sections are 305x305x198UC and external column sections are 305x305x137UC, steel S350) (Bravery, 1993). Flexible end-plates (also called header plates) were used for the beam-to-column connections and fin-plates were used for the beam-to-beam connections. In both cases S275 steel and M20, grade 8.8 bolts were used. Composite behaviour was achieved by using 19 mm diameter shear studs (with an f_u = 350 MPa) to connect the primary and secondary to the light-weight concrete and profiled metal deck composite floor slab. The geometry and measured material properties of the flooring system are summarised by Wald et al (Wald et al, 2003).

The applied load was simulated using 1 100 kg sandbags applied over an area of 18 m by 10,5 m on the floor immediately above the fire compartment. The sandbags represent 100% of the permanent actions, 100% of variable permanent actions and 56% of live actions. The applied load was designed to fail the floor, based on analytical and FE simulations. Wooden cribs with moisture content 14 % were used to provide a fire load of 40 kg/m^2.

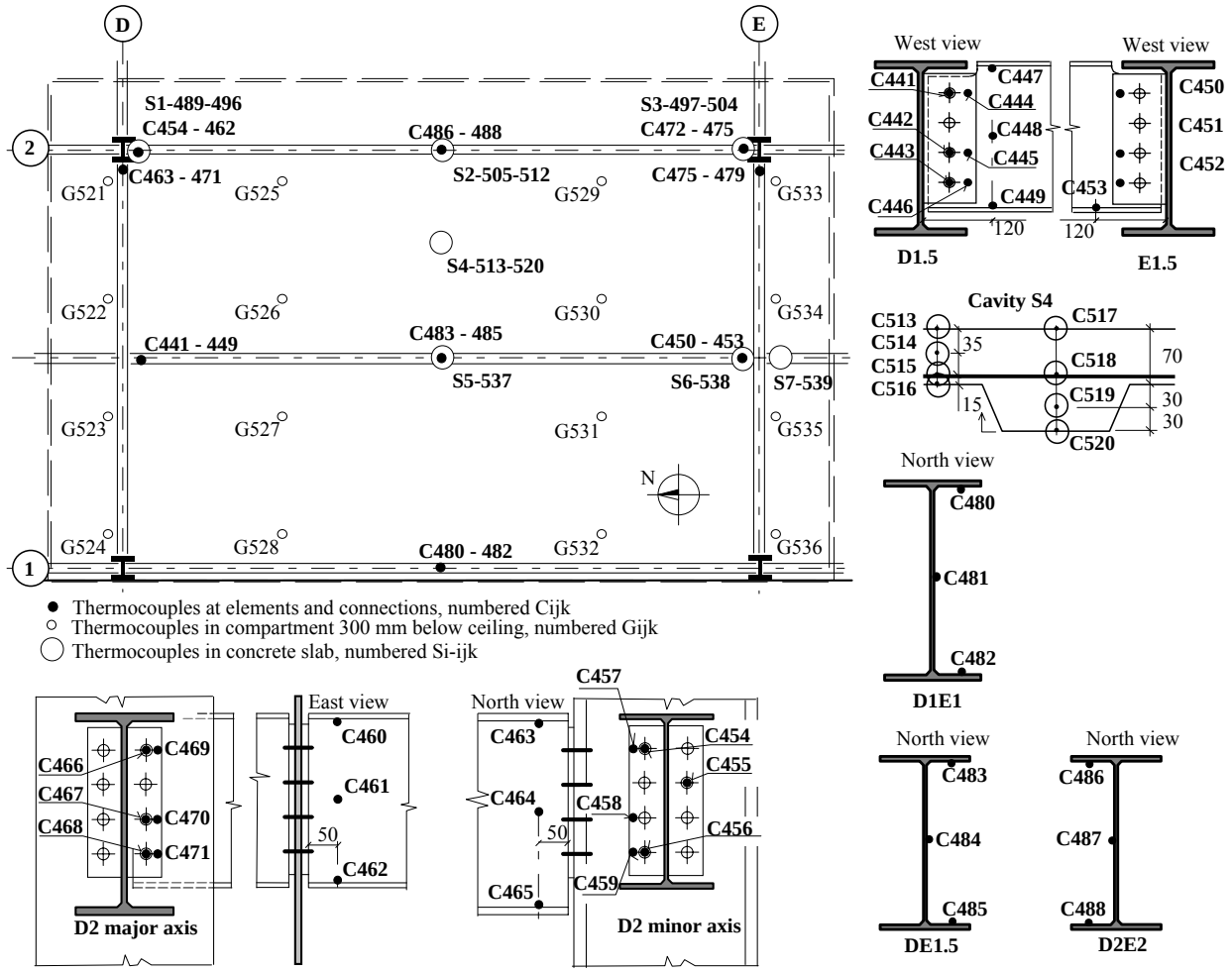

Fig. 1 Location of thermocouples in the compartment below the ceiling and on steel structure

Instrumentation

The instrumentation used included thermocouples, strain gauges and displacement transducers. A total of 133 thermocouples were used to monitor the temperature of the connections, the steel beams within the compartment, the temperature distribution through the slab and the atmosphere temperature within the compartment, see Fig.1. An additional 14 thermocouples were used to measure the temperature of the protected columns.

High and ambient temperature strain gauges were used to measure the strain in the elements. In the exposed and un-protected elements (fin plate and end plate - minor axis) nine high temperature strain gauges were used. In the protected columns and on the slab a total of 47 ambient strain gauges were installed.

Twenty-five displacement transducers were attached along the 5th floor to measure the vertical deformation of the concrete slab. An additional 12 transducers were used to measure the horizontal movement of the columns and the slab. Ten video cameras and two thermal-imaging cameras recorded the fire and smoke development and the deformations and temperature distribution (Wald et al, 2003).

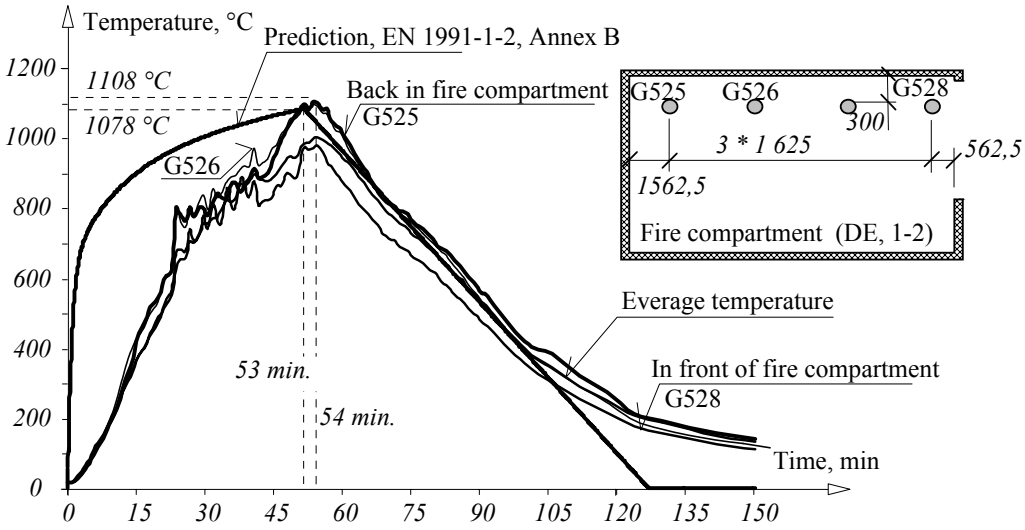

Fig. 2 Comparison of the prediction of the gas temperature to the measured temperatures

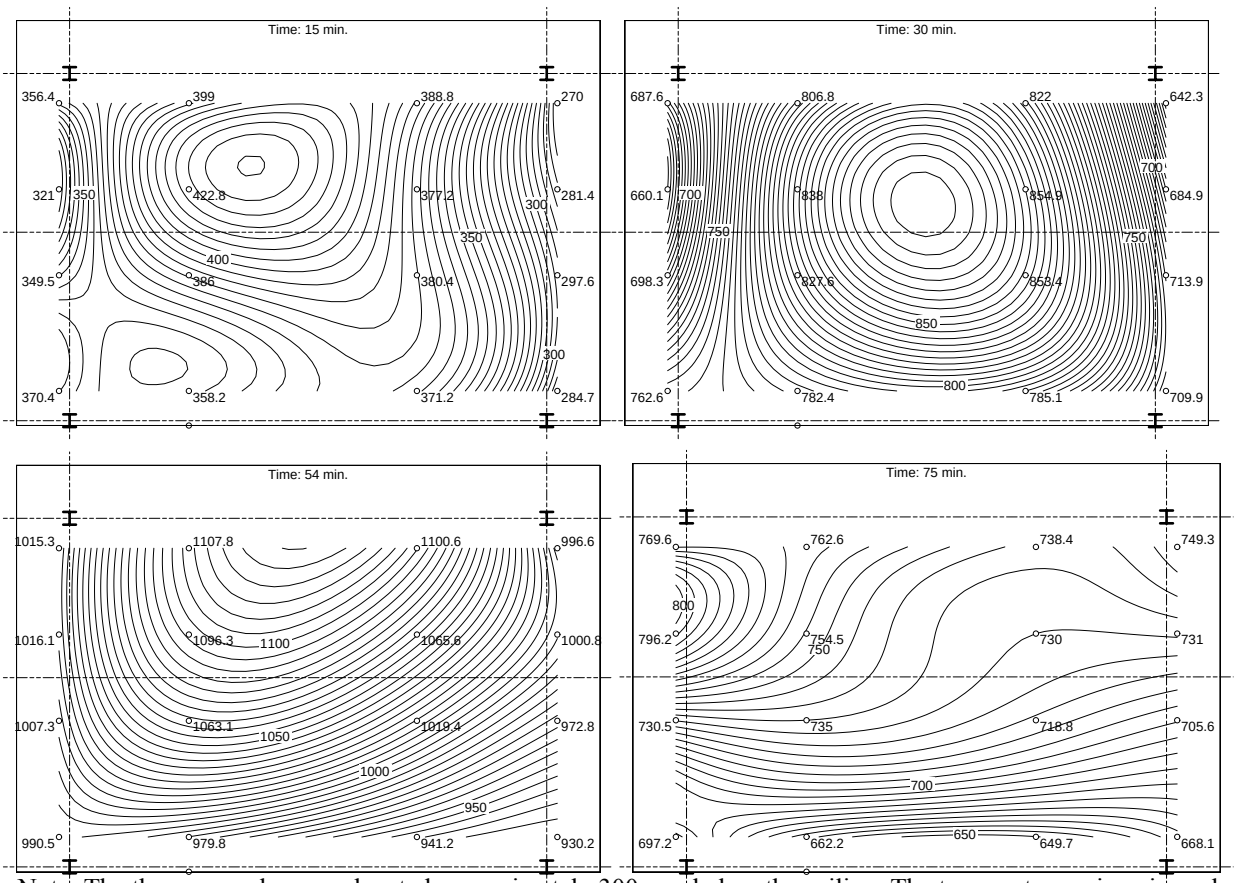

Note: The thermocouples ware located approximately 300 mm below the ceiling. The temperatures given in each of the figures represents the maximum temperature achieved between T and T-5mins. Where T is the time given in the figure.

Fig. 3 Isotherms of compartment temperatures

FIRE DEVELOPMENT AND COMPARTMENT TEMPERATURE

The quantity of fuel and the dimensions of the opening in the facade wall were designed to achieve a representative fire in an office building. Fig. 3 shows the measured time-temperature curve within the compartment. In the initial stages of the fire the temperature within the compartment grows rapidly to reach a maximum temperature of 1107,8 C after about 54 min. The maximum recorded compartment temperature occurred near the wall (2 250 mm from D2) of the compartment. Fig. 3 also compares the temperatures predicted by the parametric curve given in prEN 1991-1-2: 2003 with the test results. The parametric curve predicts a maximum temperature of 1078 °C after 53 min and this compares well with the test results, see (Wald et al, 2004). During the heating phase the isotherms shown in Fig. 3c indicate that the maximum temperatures were reached towards the back of the compartment.

The measured maximum gas temperatures are summarised in Tab. A1. The average gas temperature is average taken from all sixteen thermocouples within the compartment.

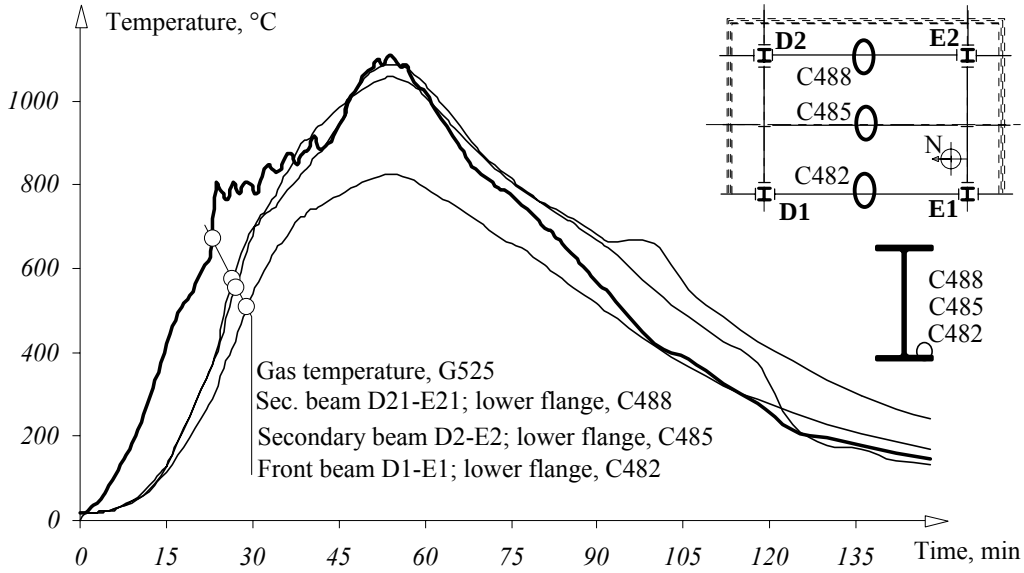

Fig. 4 Temperature variation within the beams D1-E1; D1.2-E1.2, D2-E2

BEAM TEMPERATURES

Measurements of the temperature in the mid-span beams were taken in the bottom flanges, in the web and in the upper flange. A summary of the temperatures recorded in the mid-span of the beams is given in Fig. 4. The maximum recorded steel temperature of 1087,5ºC occurred after 57 minutes in the bottom flange of the beam DE2 in the middle of the section, (see the results for thermocouple C488, in Table A2).

By using an iterative calculation procedure for the transfer of heat into the unprotected steel structure (See Expression 4.25 and B1 in prEN 1993-1-2: 2003) it is possible to predict that a maximum steel temperature of 1067 °C is reached after 54 min. This compares well with the measured data. The temperature of the beam's flanges and web can also be calculated by using clause 4.3.4.2.2 of prEN 1994-1-2: 2003 (see Buchanan 2003). The values given in Figs 3 and 4 are calculated based on measured gas temperature in thermocouple G525. The shadow effect is not taken into account.

Figure 5 compares the measured temperatures in the lower flange of the beam with a calculation procedure based on equation (B1) with a section factor for unprotected steel members $A_m / V = 208$ m^{-1} exposed on three sides. An alternative calculation procedure based on the mass of plates according to prEN 1994-1-2: 2003 is shown in Figure 6. The figure relate to a constant value for the specific heat of steel and a value varying with temperature according to 3.4.1.2 of EN 1993-1-2. A constant value for specific heat provides an acceptable but conservative solution compared to the measured data.

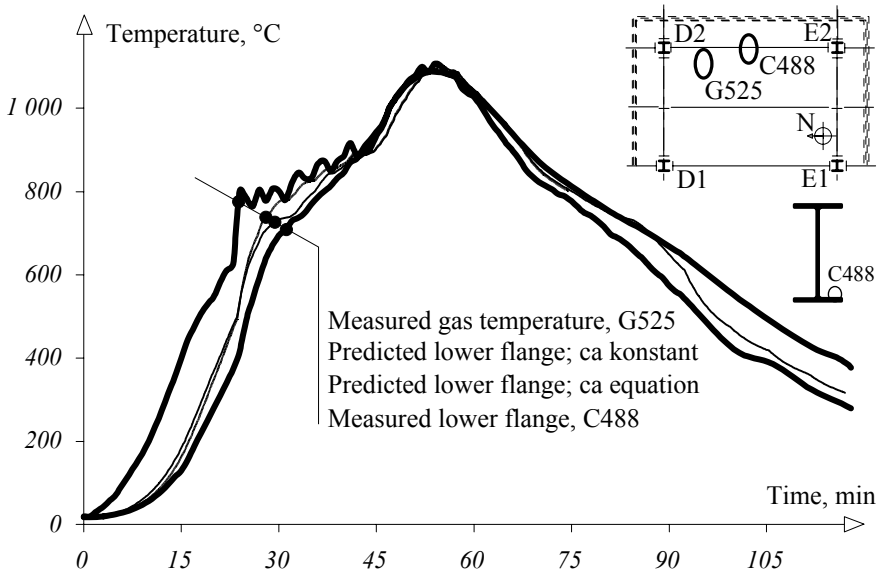

Fig. 5 Prediction of beam lower flange temperature, thermocouple C488

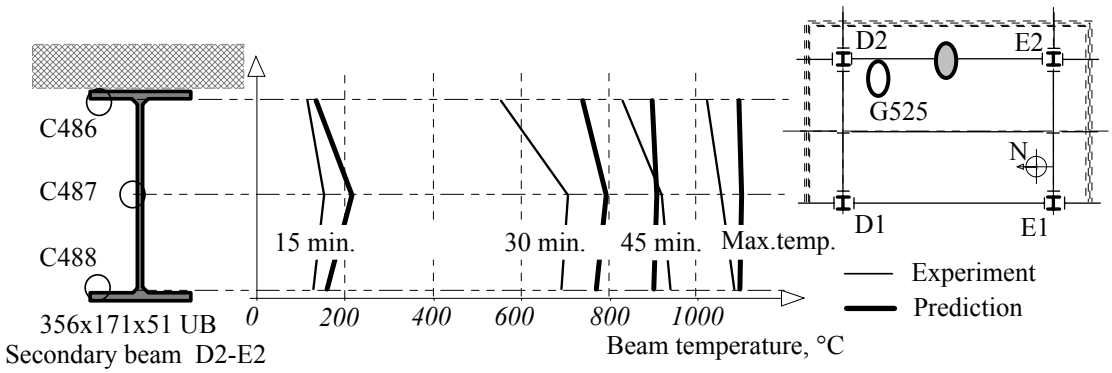

Fig. 6 Comparison of prediction to experiment; beam is calculated based on gas temperature in thermocouple G525

For Fig. 6 is applied the method in 4.3.4.2.2 of EN 1994-1-2. The web temperature calculated separately. The bottom flange section factor is based on a four sided exposure and the top flange a three sided exposure (provided at least 85% of the top flange is in contact with the slab or the voids are filled).

COLUMN TEMPERATURES

The temperatures of the columns were measured at three sections – at mid height, 500 mm from the floor, and 500 mm below the ceiling. At each section measurements were taken on both flanges and on the web. Each internal column was fire protected up to the underside of the primary beam leaving the length of column adjacent to the connection unprotected. Some of the temperatures recorded on columns D1 and D2 are presented in Fig. 7. The maximum recorded temperature in the insulated part of the column was 426,0ºC, which occurred after 106 minutes.

Once again an iterative heat transfer procedure was used to calculate the temperature of the protected column (see expression 4.27 in prEN 1993-1-2: 2003, eq (B2)). It was assumed that the fire protection material had a unit mass of $\rho_p = 310$ kg m^{-3}; a thickness of $d_p = 0{,}02$ m; a specific heat of $c_p = 1200$ J kg^{-1} K^{-1}; a thermal conductivity of $\lambda_p = 0{,}078$ W m^{-1} K^{-1}and a moisture contents p = 12 %. Fig. 8 compares the predicted and measured temperatures. Three predictions are shown in Fig. 8. These are based on the measured gas temperature in thermocouple G525, the calculated parametric temperature, see (Wald et al, 2004), and the nominal standard fire temperature. All three predictions compare reasonably well during the heating phase. However, the comparisons during the cooling phase compare less well. It is assumed that this is due to the radiation from the compartment walls which is high due to the location of the column in the rear corner of the compartment 1 m from the compartment wall.

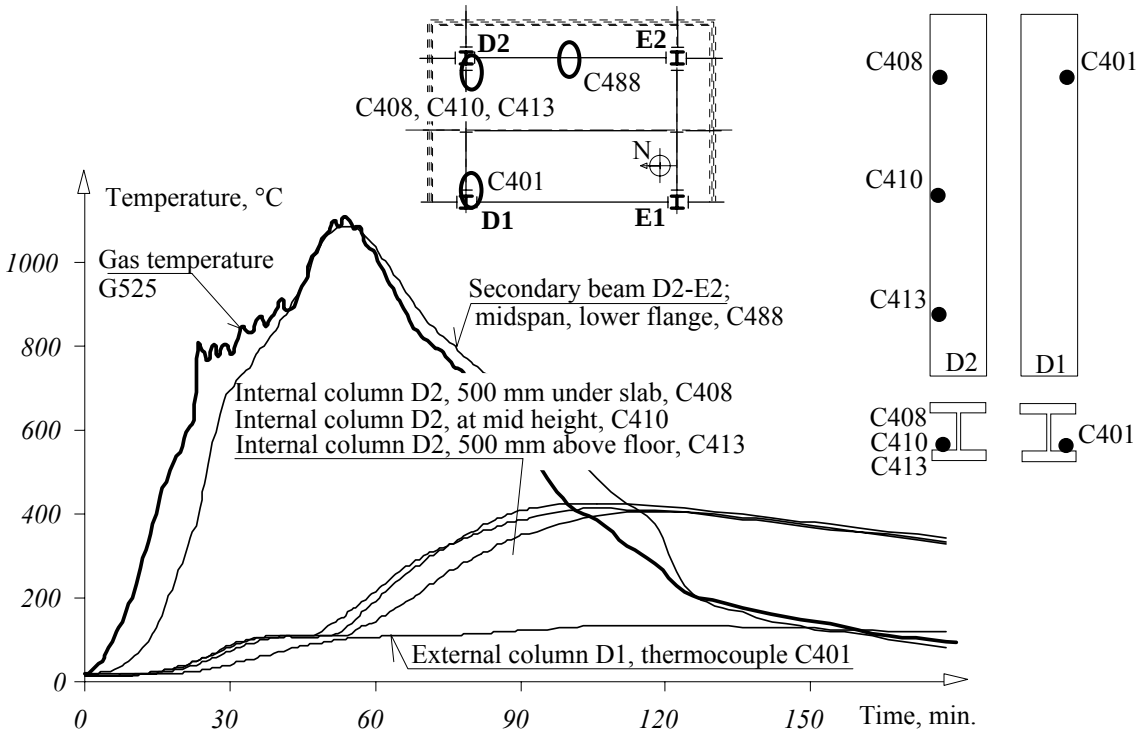

Fig. 7 Comparison of column temperature to gas and beam temperature

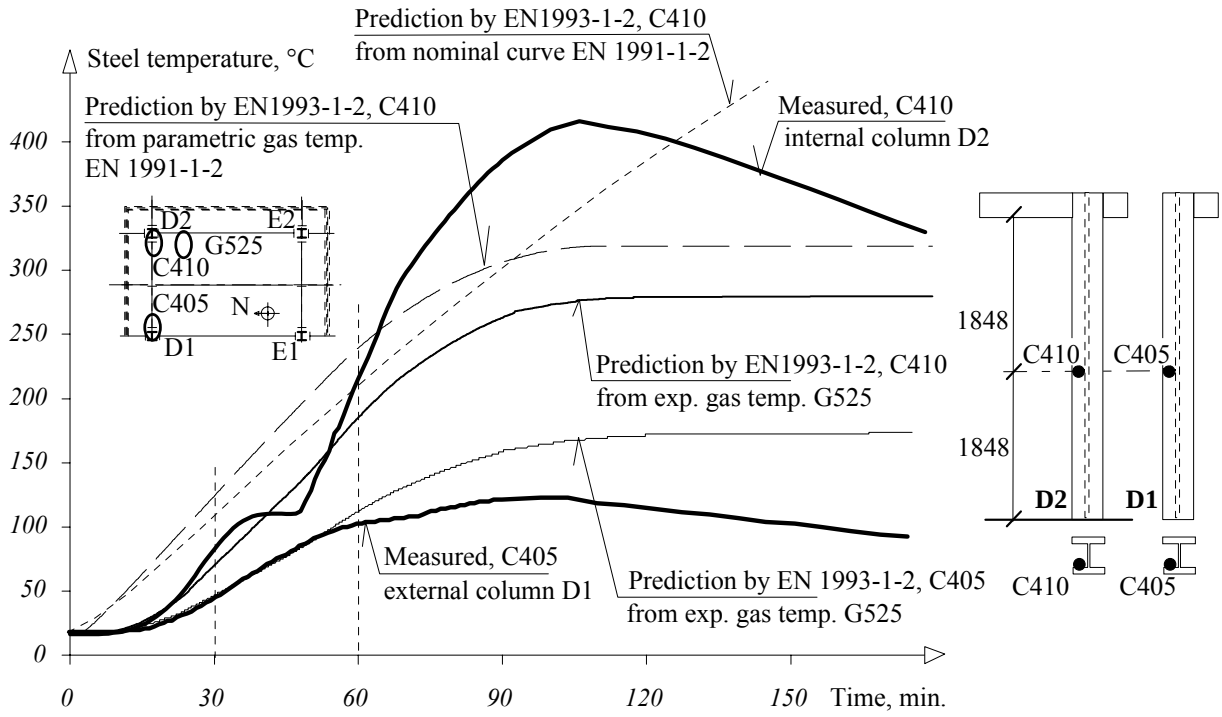

Fig. 8 Comparison of column predicted temperature to measured one, thermocouple *C408*

CONNECTION TEMPERATURES

Measurements of the temperature in the connections were taken on the beams adjacent to the connection, in the plate (end-plate or fin plate) and in the bolts, see Fig. 1. The temperatures recorded in the connections are summarised at Annex A, Table A3-A5, and presented in Fig. 9 for the beam to column minor axes connection D2-E2, in Fig. 10 for the beam to column minor axes connection D2-D1, and in Fig. 11 for the beam to beam fin plate connection D1.2-E1.2.

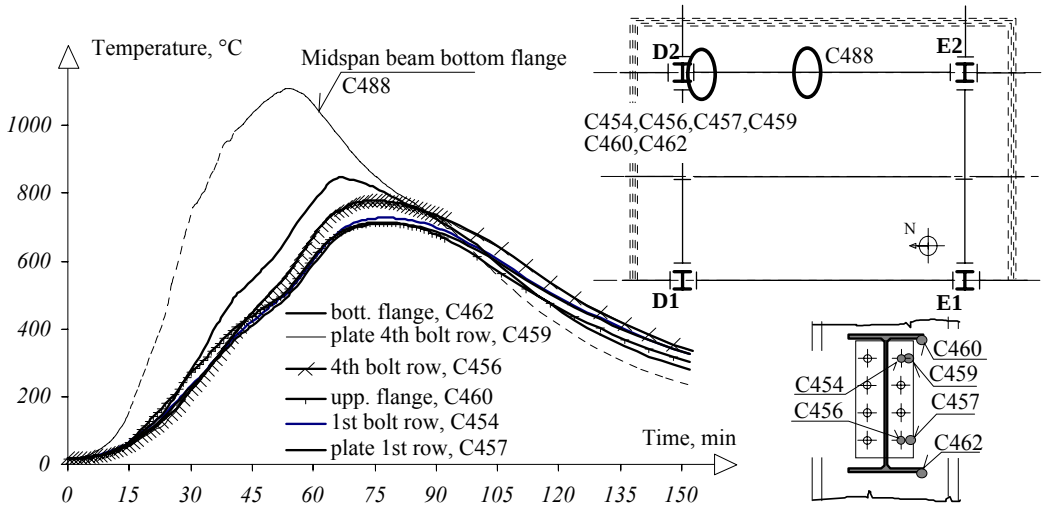

Fig. 9 Temperatures within the beam-to-column minor axes end plate connection D2-E2.

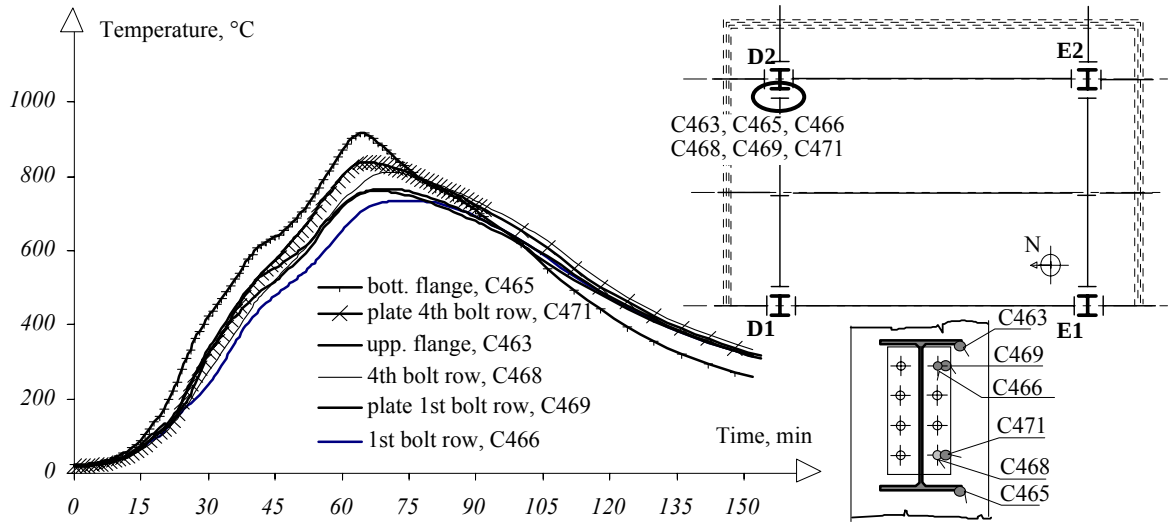

Fig. 10 Temperatures within the beam-to-column major axis end plate connection D2-D1

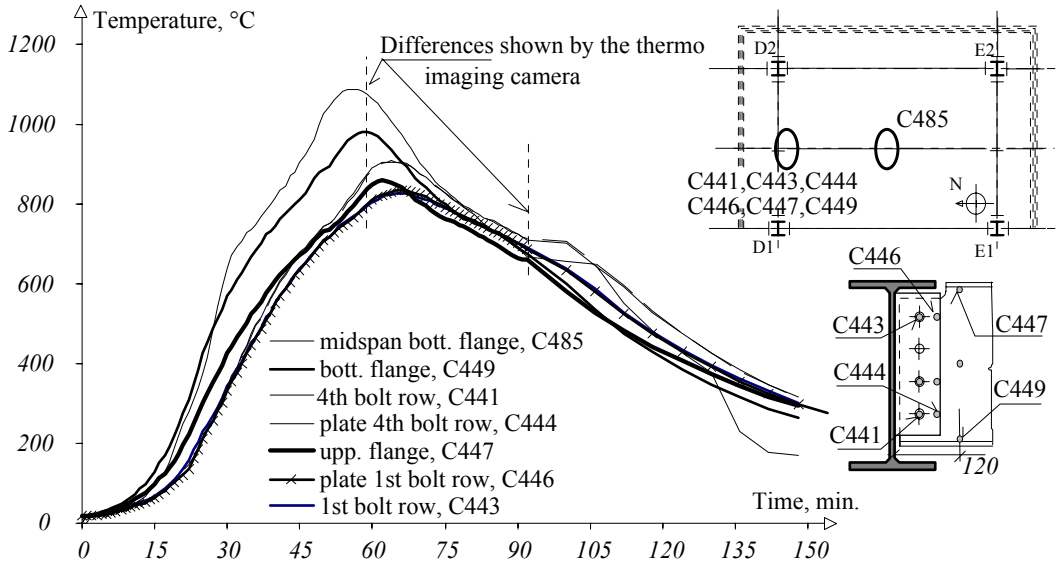

Fig. 11 Temperate at beam-to-beam fin plate connection D1.2-E1.2

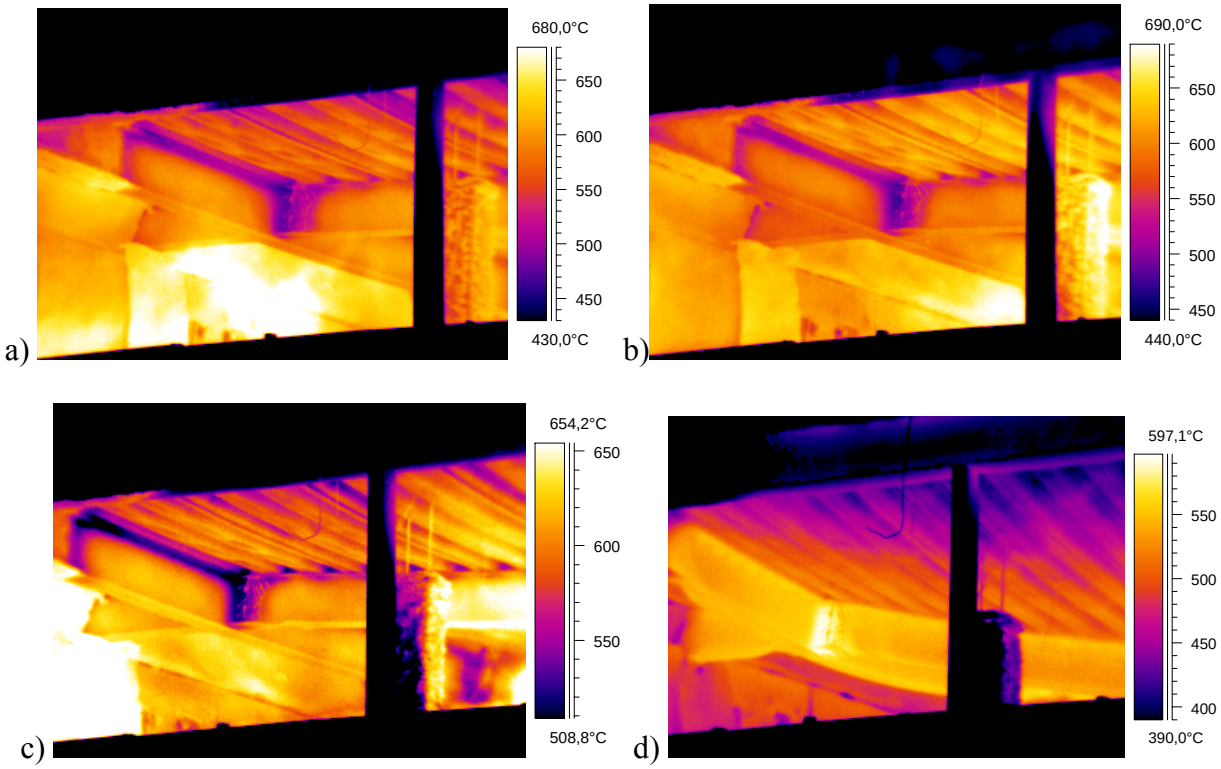

Note: Scale of colours on figures is different to visualise contours and temperatures.

Fig. 12 Fin plate connection D1.2-E1.2 recorded by thermo imaging camera a) during heating after 32 min. of fire; b) after 33 min.; c) after 35 min.; where the local buckling of lower flange is visualised and d) during cooling after 92 min.

From the experimental results, it is observed that, in the heating phase, the temperature of the joints is significantly lower than the temperature of the bottom flange of the beam measured at mid-span. This is significant as the temperature of the bottom flange of the beam is used to determine the limiting temperature of the beam and its connections. In contrast, during the cooling phase the temperature of the connection is higher than that of the beam flange. Using the thermal-imaging cameras it was possible to observe this effect, see Fig. 12 (Wald, 2004). A set of different colours is used to visualise the temperature distribution of the structure. Darker colours represent cooler areas while lighter colours represent hotter areas. In each of the figures a scale is given which relates the temperature in the structure with a different colour. The quality of the images is so good that it is possible to detect the point at which the bottom flange of the secondary beam buckled. This occurred at 32 min after the start of the test.

At the maximum atmosphere temperature, the temperature of the joints was approximately 200 ºC lower than the temperature of the beam; see Figs 7 to 9 and Table B2-B4. For all the joints tested, the temperature of the bolt row closest to the ceiling was cooler than that of the lower rows of bolts. This is due to the thermal mass of the floor slab close to the top of the connection. prEN 1993-1-2: 2003 recognises this effect and contains a set of recommendations for calculating the temperature distribution in an end-plate connection. The effect that the thermal mass of the floor slab has on the temperature distribution of a connection is illustrated in Figs. 7 to 9 for the joints tested. prEN 1993-1-2: 2003 gives two methods for calculating the temperature of a connection. These approaches are briefly explained below:

- The first is based on the concentration of mass in the connected parts (see expression D3.1(1)),
- The second applies where the beams are supporting concrete slabs. In this case simplified expressions are given for calculating the temperature distribution in the connection based on the temperature of the bottom flange of the supported beam at mid-span, see expression D3.1(4).

The predictions by both methods are based on the measured steel temperature and are compared to the experimental results for the beam-to-column minor axes end plate connection D2-E2 in Fig 11. The local concentration of mass was calculated using two different approaches. The first approach is based on the thickness and additional front surface (A_m/V = 141 m^{-1}) of the end-plate and column web while the second is based on the cumulated thickness of the end-plate and column web and the additional front surface (A_m/V = 92 m^{-1}).

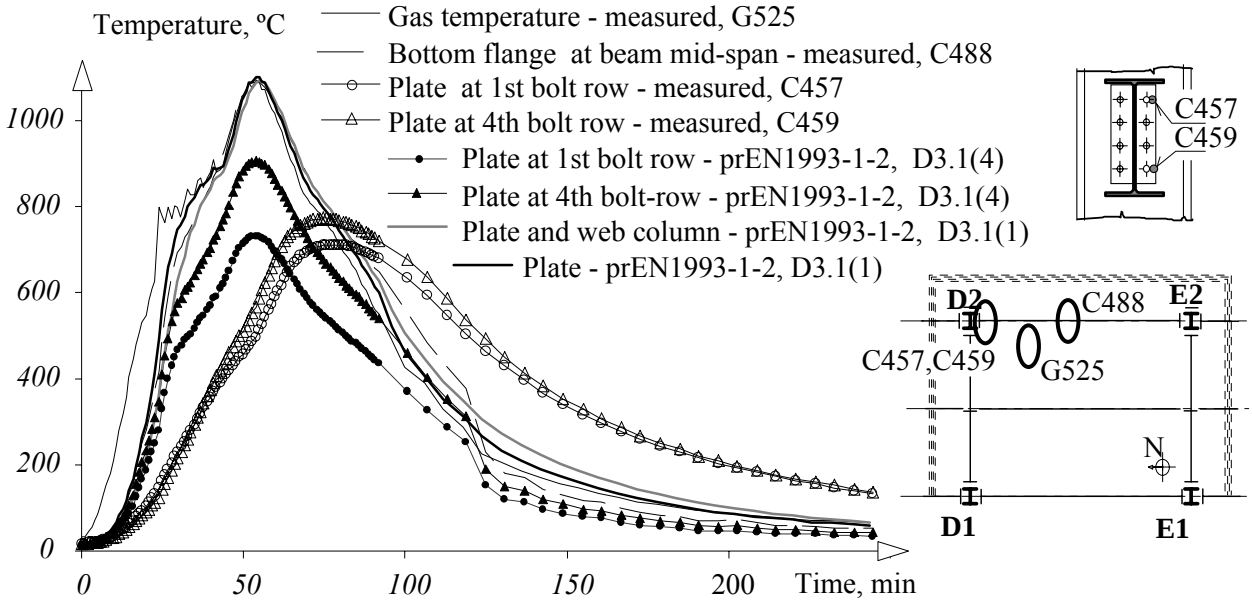

Fig. 13 Comparison of the prediction of temperatures within the beam-to-column minor axes end plate connection D2-E2 to experiment

It is observed that with both approaches, the maximum temperatures are higher than the test values and occur at approximately the same time. During the cooling phase, the calculated end-plate temperatures are lower than the experimentally observed temperatures. Comparing both analytical approaches, the method based on the local mass by section factor is more conservative than the simplified expressions. These results supports a numerical study carried out by Franssen et al (Franssen and Brauwers 2002) that shows that prEN1993-1-2: 2003 gives conservative values during the cooling phase.

For the fin plate connection D1.2-E1.2 the predictions are compared to the test results in Fig. 14. The predictions are based on the temperature of the lower flange of the beam, on the gas temperature and A_m/V = 204,6 m^{-1} with the mass of the fin plate and web A_m/V = 128,8 m^{-1}. The prediction based on the measured temperature of the beam bottom flange at mid-span is used to predict the temperature of the fin plate at the level of the fourth bolt row.

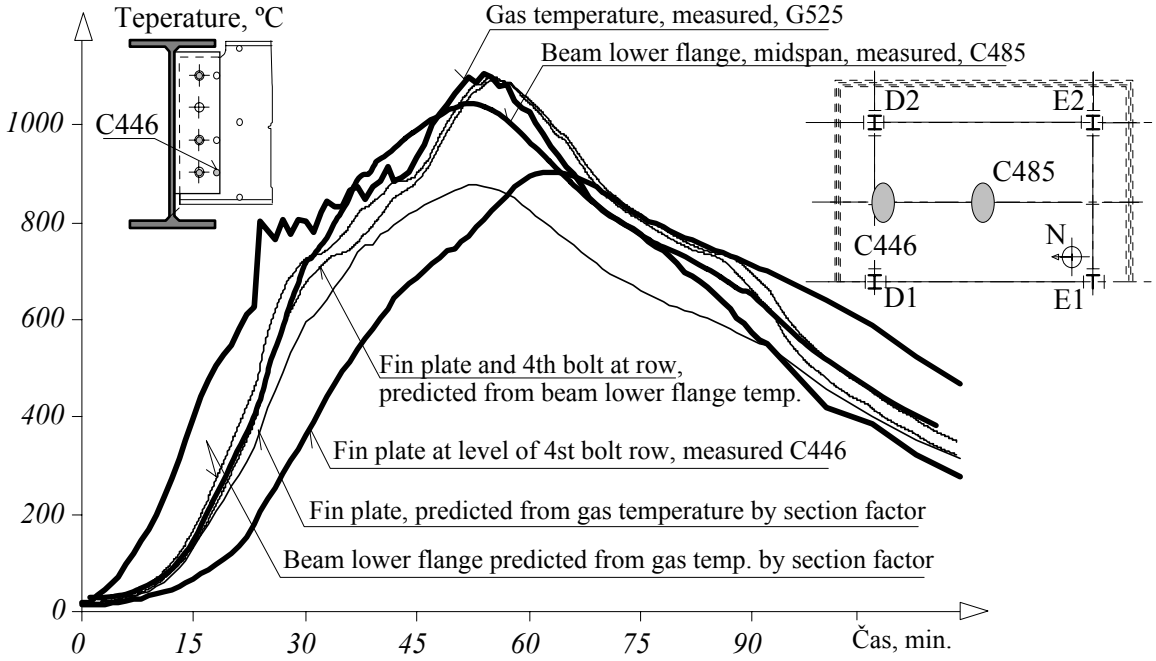

Fig. 14 Comparison of the prediction of temperatures within the beam-to-beam fin plate connection D1.2-E1.2 to experiment

COMPOSITE SLAB TEMPERATURES

Slab temperatures were measured in seven locations as shown in Fig. 1. In locations S1 - S4 temperatures were measured in the ribs on the lower surface of the metal decking (0 mm), in the concrete 30 mm above the metal decking, on the reinforcement approximately 75 mm above the metal decking and on the upper surface of the concrete 130 mm above the metal decking. Temperatures were also measured next to the ribs on the lower surface of the metal decking (0 mm), in the reinforcement approximately 15 mm above the metal decking, in the concrete 35 mm above the metal decking and on the upper surface of the concrete 70 mm above the metal decking. The temperature of the reinforcement was measured in the ribs at locations S5 - S7.

Temperature measurements on the lower surfaces of the slab were limited because the thermocouples were connected to the metal sheeting, which debonded from the concrete in the first 20 to 30 min of the test. Maximum temperatures in the middle of the slab next to the rib (35 mm) and in the middle of the rib (30 mm) were very similar - up to 250°C in a 100 - 150 minutes, see Fig. 15. The temperatures of the reinforcement in the rib are different to those measured next to the rib see Fig. 16. This is because of the different amounts of concrete cover. Figure 17 shoes that the temperature of the reinforcement over the rib is higher than the temperature of surrounding concrete. The temperatures of the upper surfaces of the concrete over the rib and the upper surface of the concrete next to the rib are similar with maximum temperatures of approximately 110°C, see Fig. 18.

A summary of the temperatures recorded in the slab at location S4 is presented in Fig. 17. It shows that the temperatures of the reinforcement over the rib were less than 150 °C.

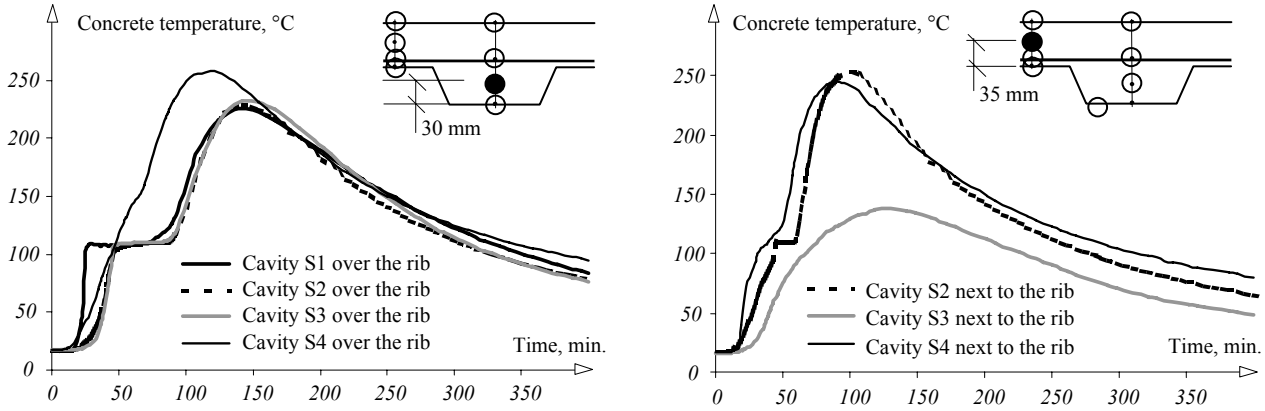

Fig. 15 Temperatures in the middle of the rib and in the middle height next to the rib

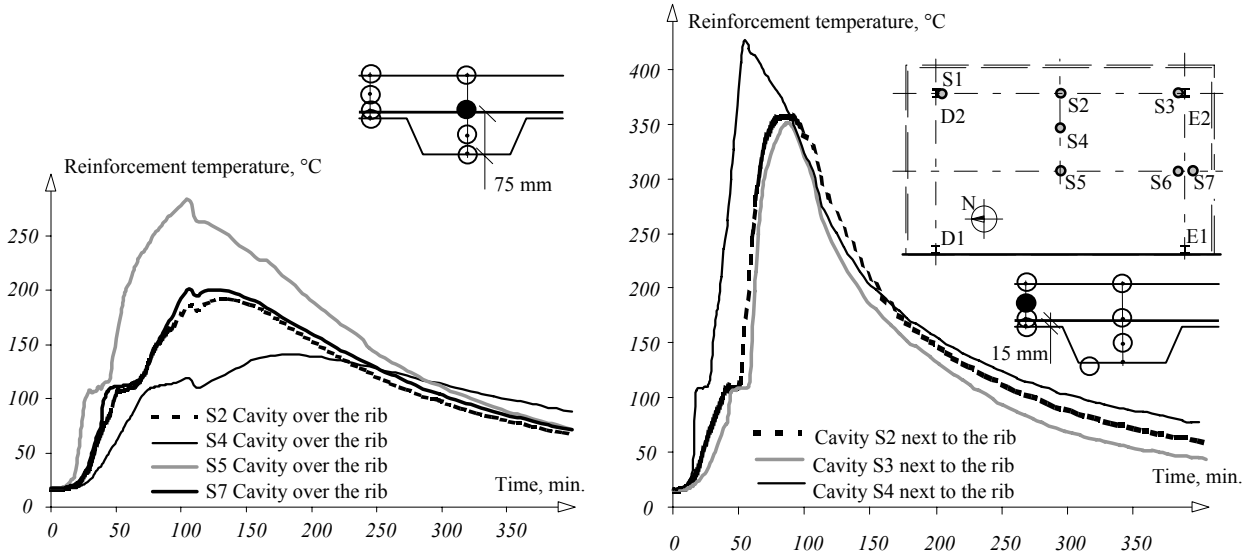

Fig. 16 Temperatures of the reinforcement over the rib and next to the rib

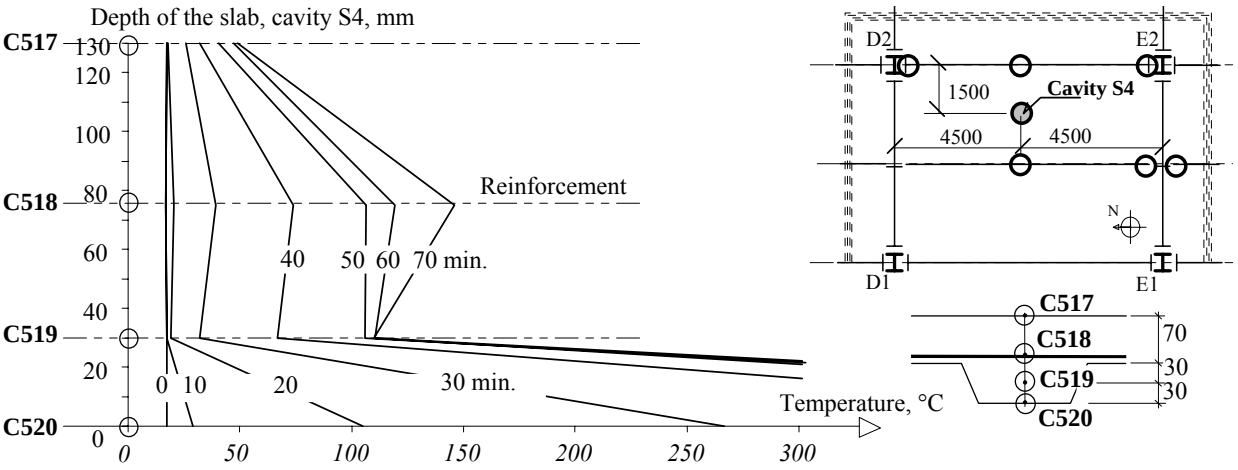

Fig. 17 Temperature variation within slab over the rib, cavity S4

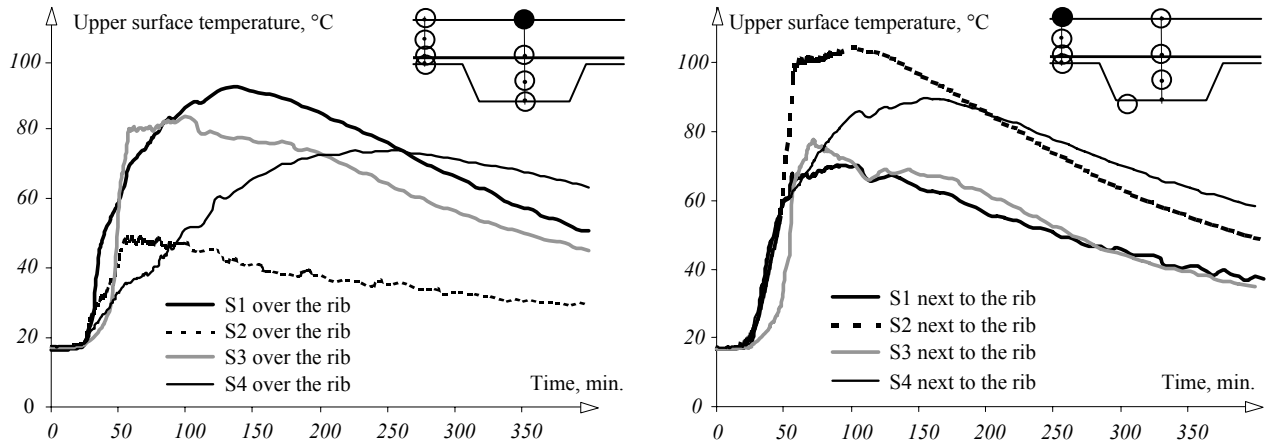

Fig. 18 Temperatures of the upper surface over the rib and next to the rib

The calculation of temperature in the concrete slab is complex compared to the procedure for calculating the steel temperatures. Because of the massive sections of concrete (compared with steel) and the thermal properties of concrete it is not possible to calculate the temperatures by using a simple analytical equation. However, the temperatures in concrete could be calculated by FEM or by using a differential method. Table D.5 of prEN 1994-1-2: 2003 contains the temperatures for normal weight concrete subject to a standard time-temperature curve temperature for fire duration from 30 to 240 minutes. This table can also be used for lightweight concrete. For the preliminary prediction of the slab temperatures in this test the differential method according to Karpas (Karpaš, Zoufal 1989) was used (see Annex C of this paper). The temperatures can be calculated using a spreadsheet.

The results from the differential method depend on several parameters. One of the parameters that has a significant effect is the moisture content of the concrete. The moisture content of the concrete causes a plateau in the heating curve when temperatures of 100°C are reached (Figs 15 and 16). Figs 19 and 20 show the temperatures of the concrete slab next to the rib as a function of moisture content and are compared with the measured values. From measurements it is reported that the moisture content in the concrete of floors in the Cardington frame is approximately 3 %.

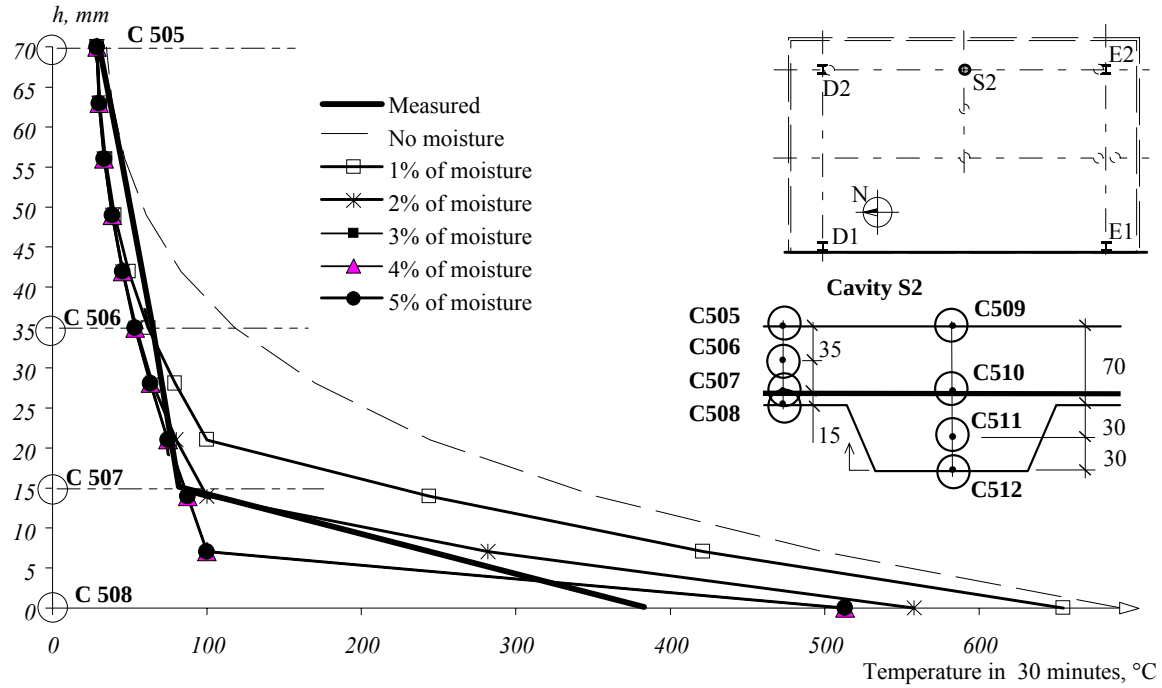

Fig. 19 Influence of the concrete moisture on slab temperatures across the height in 30 min., cavity S2

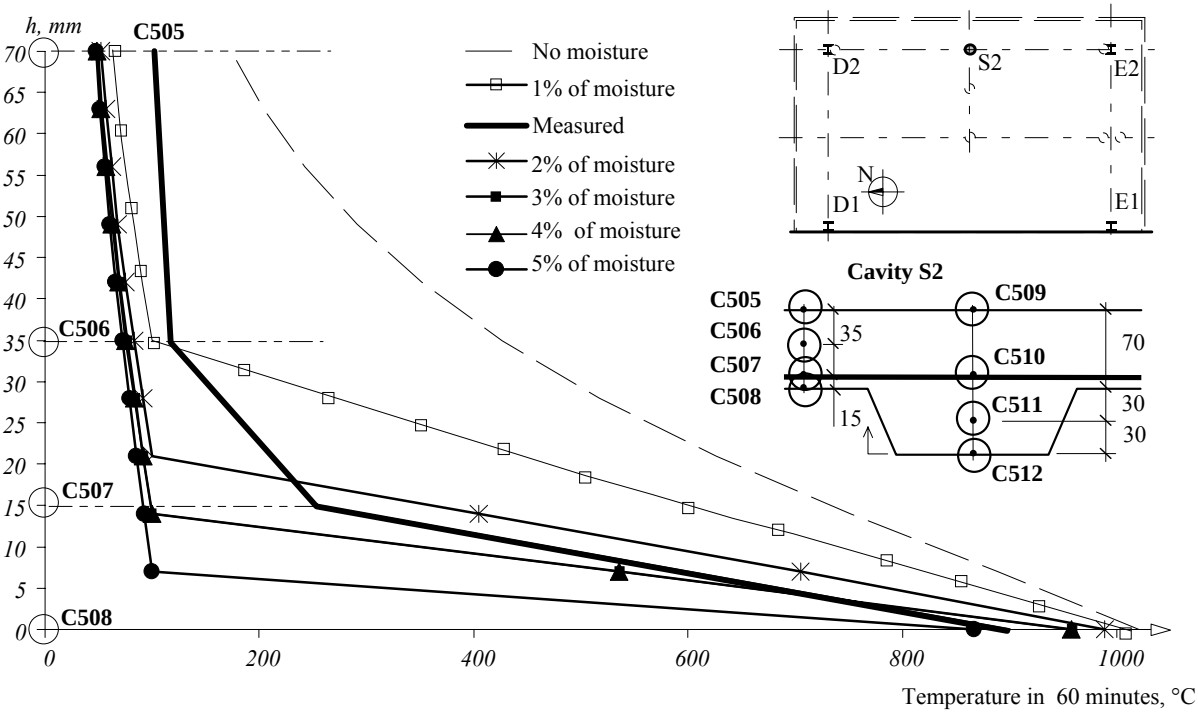

Fig. 20 Influence of the concrete moisture, cavity S2, slab temperatures across the height in 60 minutes

The predicted temperatures of the concrete slab are based on a parametric time- temperature curve (Wald et al, 2003) and are compared with the measured values. The results of calculations

based on the temperatures obtained from nominal parametric fire curve and those obtained from the measured gas temperatures are shown in Fig. 21 and Fig. 22. The convection and radiation components of heat transfer coefficients (Annex C, Table C.1) have a significant influence on modelling.

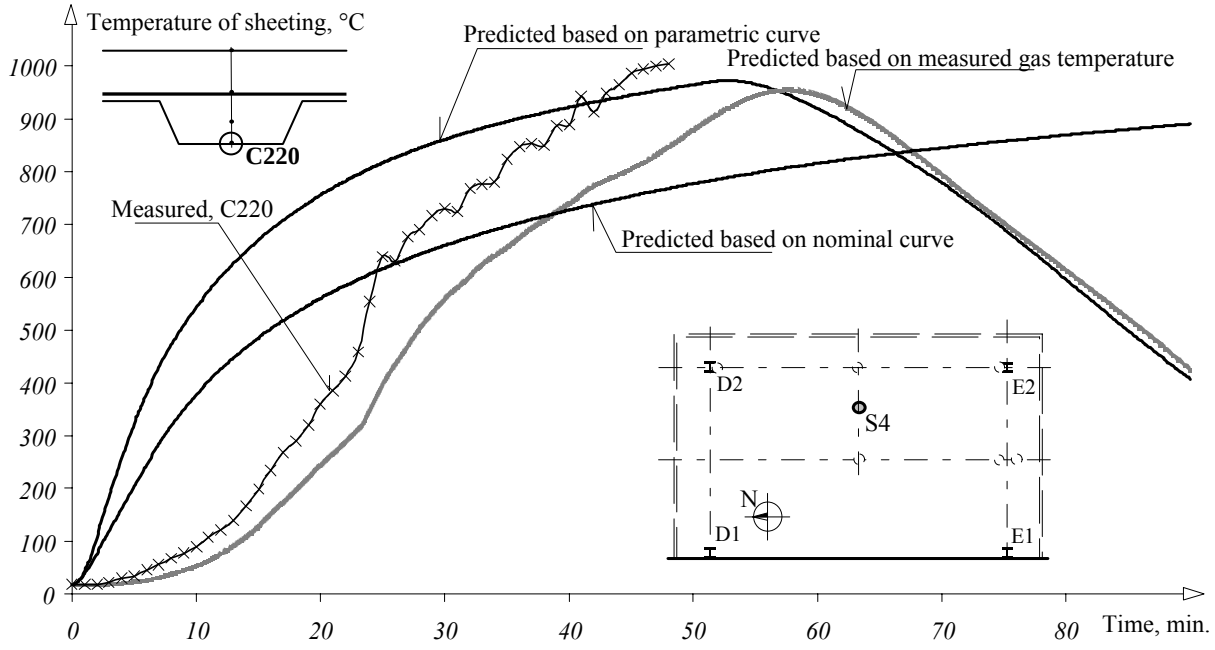

Fig. 21 Comparison of predicted and measured temperature at the cavity S4, bottom of the rib 0 mm, thermocouple C220

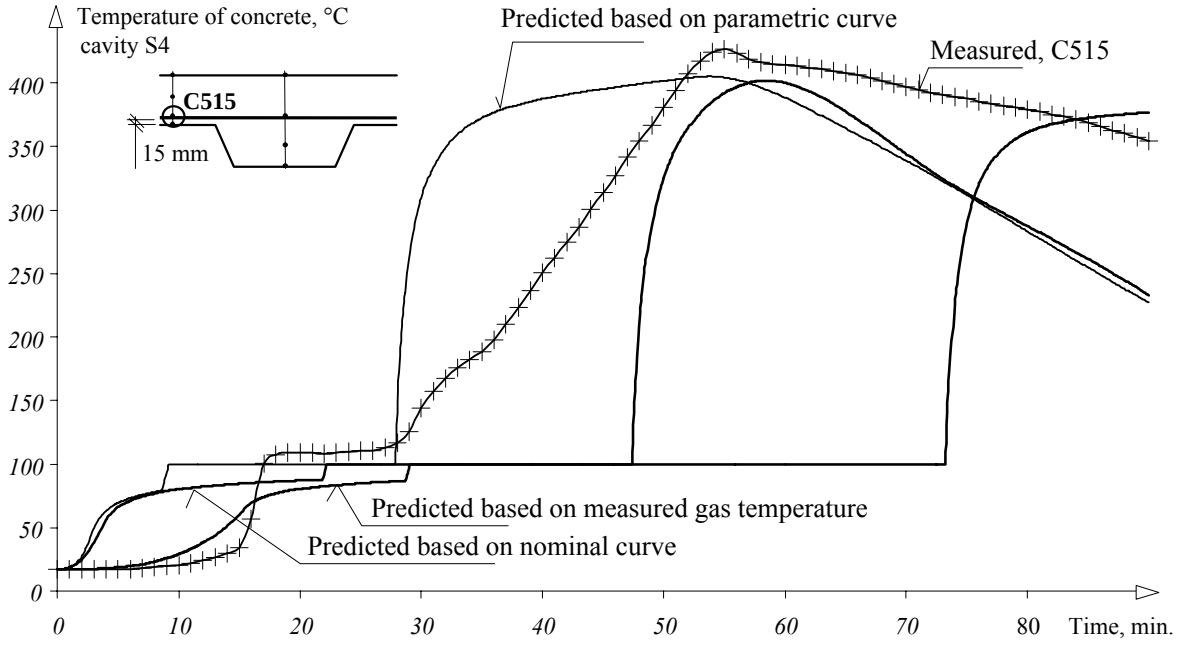

Fig. 22 Comparison of prediction of temperature according to different time-temperature curves to experiment, cavity S4 next to rib 15 mm from bottom, thermocouple C515

CONCLUSIONS

On the 16 January 2003 a full-scale fire test was carried out at the Building Research Establishment's Cardington laboratory. One of the main aims of this fire test was to collect high quality data on the distribution of temperatures within the main structural members. This paper presents an overview of the Cardington facility together with a description of the fire test. It also presents in detail the measured temperatures in the composite steel/concrete slab, the supporting steel beam and columns and in the beam-to-column and beam-to-beam connections. Comparison is also made with the analytical methods given in prEN 1993-1-2: 2003 for calculating the temperature and temperature distributions in the structural steel members. From these comparisons it can be concluded that:

The methods for calculating the compartment temperature given in prEN 1991-1-2: 2003 compare well with the measured data (Wald et al, 2004). The incremental analytical models predict the temperatures of the unprotected beams with a good accuracy. The column temperature may be predicted from the gas temperature during the heating phase, for the first 60 minutes of fire, by 2D incremental analytical models which also apply to the columns with the unprotected joint area.

Calculating the temperature of the connections using the measured gas temperature in the fire compartment (based on the mass of the connection parts) during the heating phase is conservative, see Figs 11 and 12. However, a calculation based on the bottom flange temperature of the supported beam is less conservative. The analytical prediction of the temperature of the structure during its cooling will help in the next revision of the standard prEN 1993-1-2: 2003 to apply the available knowledge with higher accuracy bringing high safety and economy.

The temperatures of the concrete slab are lower than the temperatures of the supporting steel members. The accuracy of the methods for calculating the temperature of the concrete slab is sensitive to the moisture content of the concrete.

ACKNOWLEDGEMENT

The authors of this paper would like to thank all nineteen members of the project team who worked on this large scale experiment from October 2002 to January 2003. Special thanks go to Mr. Nick Petty, Mrs. Petra Studecká and Mr. Martin Beneš for careful measurement of data presented above. This paper was prepared as a part of project COST C12.

REFERENCES

Bailey C.G., Lennon T., Moore D.B. (1999), "The behaviour of full-scale steel-framed building subject to compartment fires" *The Structural Engineer*, Vol.77/No.8, p. 15-21.

Bravery P.N.R. (1993), "*Cardington Large Building Test Facility, Construction details for the first building*" Building Research Establishment, Internal paper, Watford, p. 158.

Buchanan A.H. (2003), "*Structural design for fire safety*" John Wiley & Sons, Chichester, ISBN 0-471-89060-X.

ENV 1994-1-2: 1994, Eurocode 4: Design of composite steel and concrete structures, Part 1.2 General rules "*Structural Fire Design"* CEN, European Committee for Standardization, Brussels.

Franssen, J.M., Brauwers, L. (2002), "Numerical determination of 3D temperature fields in steel joints", *Proc. of Second International Workshop "Structures in Fire"*, Christchurch, March 2002.

Lennon T. (1997), "*Cardington fire tests: Survey of damage to the eight storey building*", Building Research Establishment, Paper No127/97, Watford, p. 56.

Karpaš J., Zoufal R. (1989), "*Požární odolnost ocelových a železobetonových konstrukcií*" *("Fire Resistance of Steel and Concrete Structures")*. Zabraňujeme škodám, Svazek 28. Česká státní pojišťovna, Praha 1989.

Moore D.B. (1995), "*Steel fire tests on a building framed*". Building Research Establishment, Paper No. PD220/95, Watford, p. 13.

Moore, D. B, Nethercot, D, A and Kirby, P. A. (1993), "Testing Steel Frames at Full Scale", *The Structural Engineer* 71 Nos. 23 & 24, December.

Pettersson O., Magnusson S. E., Thor J. (1976), "*Fire Engineering Design of Steel Structures*". Publication 50. Swedish Institut of Steel Construction, Stockholm. Sweden.

prEN 1991-1-2: 2003, Eurocode 1: Actions on structures, Part 1-2: General actions – "*Actions on structures exposed to fire*". Final Draft, CEN, European Committee for Standardization, Brussels, April.

prEN 1993-1-2: 2003, Eurocode 3: Design of steel structures, Part 1.2 General rules "*Structural Fire Design"* CEN, European Committee for Standardization, Brussels, stage 49 draft November.

prEN 1994-1-2: 2003, Eurocode 4: Design of composite steel and concrete structures, Part 1.2 General rules "*Structural Fire Design"* CEN, European Committee for Standardization, Brussels, stage 34 draft May.

Steel Structures Research Committee (1931, 1934, 1936), *First, second and third reports*; Department of Scientific and industrial Research, London, HMSO.

Wang Y.C. (2002), "*Steel and composite structures"* Behaviour and design for fire safety, Spon Press, London, ISBN 0-415-24436-6.

Wald F., Simões da Silva L., Moore D., Santiago A. (2004), Experimental Behaviour of Steel Joints under Natural Fire in "*Proceedings of ECCS and AISC meeting*" Amsterdam, in press.

Wald F., Silva S., Moore D.B, Lennon T. (2004), Structural integrity fire test, in "*Proceedings Nordic Steel Conference"*, Copenhagen, in press.

Wald F., Silva S., Moore D.B, Lennon T., Chladná M., Santiago A., Beneš M. (2004), Experiment with structure under natural fire, *The Structural Engineer*, in press.

Wald F., Santiago A., Chladná M., Lennon T., Burges I., Beneš M. (2003) "*Tensile membrane action and robustness of structural steel joints under natural fire*" Part 1 - Project of Measurements; Part 2 – Prediction; Part 3 – Measured data; Part 4 – Behaviour, Internal report, BRE, Watford.

Annex A
MEASURED TEMPERATURES

Tab. A1 Maximum gas temperatures in time intervals °C, thermocouples 300 mm under ceiling, numbers see Fig. 1

Thermocouple Time interval, min.	**C 521**	**C 522**	**C 523**	**C 524**	**C 525**	**C 526**	**C 527**	**C 528**	aver.
10 – 15	356,40	321,00	349,50	370,40	399,00	422,80	386,00	358,20	373
25 – 30	687,6	660,1	698,3	762,6	806,8	838	827,6	782,4	805
40 – 45	810,5	777,3	834,8	851,1	935,0	971,6	964,5	885,9	966
0 – 180	1 015,3	1 016,1	1 007,3	990,5	1 107,8	1 096,3	1 063,1	979,8	1 074
75 – 80	769,6	796,2	730,5	697,2	762,6	754,5	735,0	662,2	761
90 – 95	567,1	579,7	576,9	528,7	560,3	535,0	555,1	475,1	555

Tab. A2 Steel beam temperatures °C, thermocouples numbers see Fig. 1

Thermocouple Time, min.	**C 480**	**C 481**	**C 482**	**C 483**	**C 484**	**C 485**	**C 486**	**C 487**	**C 488**
15	65,7	115,0	115,6	102,4	137,8	156,0	115,7	153,5	129,4
30	390,4	541,5	539,7	503,0	696,2	720,7	556,3	709,0	694,6
45	708,5	756,8	775,5	833,2	966,1	995,6	832,8	923,0	942,9
60	792,1	776,9	792,7	958,6	966,5	995,1	1 007,4	1 007,2	1 037,8
Max.	798,4	810,9	824,5	981,7	1 032,4	1 057,4	1 025,7	1 057,6	1 087,5
75	681,5	636,9	658,0	795,0	770,5	797,2	835,5	801,0	813,3
90	544,3	489,4	505,6	683,1	633,7	662,2	709,0	661,9	658,1
106	419,9	362,6	368,4	533,7	468,5	485,1	559,5	495,1	484,8
130	286,7	230,4	227,7	359,4	296,9	297,6	364,3	310,5	179,1
Position	Upper flange	Beam web	Lower flange	Upper flange	Beam web	Lower flange	Upper flange	Beam web	Lower flange

Tab A3 Temperatures °C, header plate connection D2-C2, minor axis, , thermocouples numbers see Fig. 1

Thermocouple Time, min.	**C 454**	**C 455**	**C 456**	**C 457**	**C 459**	**C 460**	**C 461**	**C 462**
15	67,0	48,5	58,5	62,1	55,1	66,9	61,3	63,1
30	233,0	187,4	220,9	231,2	216,7	270,9	273,0	281,3
45	422,0	386,5	447,7	410,1	446,2	439,0	491,8	545,0
60	601,5	623,5	672,7	589,3	673,9	608,7	706,3	774,0
75	726,4	743,2	779,1	708,9	772,2	713,4	779,4	816,3
Max.	728,0	745,3	779,1	711,1	772,2	714,4	780,9	846,7
90	699,6	719,0	735,2	687,5	731,6	679,1	726,3	725,9
106	596,2	620,1	635,4	591,8	637,2	564,1	616,5	583,6
130	431,5	440,8	450,4	429,0	451,0	401,7	429,4	383,9
160	297,1	301,2	305,2	296,8	306,4	277,8	288,3	253,5
Position	1st bolt	2nd bolt	4th bolt	Plate 1st row	Plate 4th row	Upper flange	Web	Lower flange

Tab. A4 Temperatures °C, at header plate connection D2-D1, major axis, thermocouples numbers see Fig. 1

Thermocouple Time, min.	**C 466**	**C 467**	**C 468**	**C 469**	**C 470**	**C 471**	**C 463**	**C 464**	**C 417**
15	67,4	60,8	61,4	74,1	68,2	67,3	64,0	100,1	89,4
30	241,2	270,4	274,0	319,5	324,0	323,9	334,4	470,1	422,8
45	476,8	512,8	519,4	516,7	567,9	572,5	553,5	654,2	636,5
60	655,3	713,4	735,7	717,6	785,9	800,9	724,0	881,0	870,5
75	733,2	797,9	804,3	758,8	808,2	808,3	747,7	798,8	818,8
Max.	733,8	800,0	811,7	765,8	831,3	838,6	762,0	905,5	916,0
90	692,7	734,7	734,8	691,5	730,3	723,5	679,4	687,9	709,4
106	581,3	631,6	628,5	583,3	619,1	608,1	567,4	540,1	552,1
130	412,1	433,2	435,8	415,6	427,0	423,6	408,7	365,6	354,5
160	284,9	299,8	305,2	290,0	297,7	296,2	289,9	253,4	233,8
Position	1st bolt	3rd bolt	4th bolt	Plate 1st row	Plate 3rd row	Plate 4th row	Upper flange	Web	Lower flange

Tab. A5 Temperatures °C, at fin plate connection D1.2-E1.2, thermocouples numbers see Fig. 1

Thermocouple Time, min.	**C 441**	**C 442**	**C 443**	**C 444**	**C 446**	**C 447**	**C 448**	**C 449**
15	68,5	66,4	70,2	65,6	70,5	98,2	85,9	129,5
30	343,0	350,1	367,6	331,1	368,8	424,5	425,5	570,0
45	636,3	671,5	686,9	635,8	691,6	671,2	726,5	812,4
60	805,3	862,9	894,5	810,3	899,1	848,6	912,9	975,5
Max.	825,6	881,4	907,2	834,3	908,3	859,1	913,8	981,6
75	789,1	810,8	817,4	792,9	816,4	764,0	784,7	798,3
90	703,6	717,0	718,8	702,0	716,7	663,9	686,7	692,0
106	587,0	598,4	597,1	580,7	591,1	527,5	542,4	534,7
130	396,2	391,4	382,9	390,6	383,9	373,6	362,1	346,9
160	257,1	249,2	242,1	254,1	244,1	257,9	236,8	225,5
Position	1st bolt	3rd bolt	4th bolt	Plate. 1st row	Plate. 4th row	Upper flange	Web	Lower flange

Tab. A6 Temperatures °C, in slab, cavities S2 and S4, thermocouples numbers see Figs 1 and 17

	Cavity S4, next to the rib			Cavity S4, across the rib				Cavity S2, across the rib			
Time, min	**C 513**	**C 514**	**C 515**	**C 517**	**C 518**	**C 519**	**C 520**	**C 509**	**C 510**	**C 511**	**C 512**
15	17,3	19,0	34,5	17,5	17,1	21,1	199,3	17,5	17,9	17,6	52,6
30	27,5	94,3	144,1	21,6	25,3	54,2	731,5	25,7	39,2	32,2	266,5
45	53,6	117,9	313,7	30,0	50,8	102,8	986,6	36,9	84,7	100,9	661,8
60	64,3	185,1	413,9	36,2	81,1	142,5	*	48,4	109,6	109,1	936,5
75	73,3	233,6	387,6	38,8	108,7	182,8	*	47,5	134,6	110,1	776,3
90	80,3	245,1	354,2	45,5	113,1	230,7	*	46,4	162,4	113,7	667,1
Max	89,7	245,3	426,7	74,0	140,4	257,9	1022,8	48,8	192,1	228,9	1040,6
106	86,0	237,4	307,2	52,0	118,9	255,5	*	45,1	185,8	163,6	*
130	87,0	209,9	237,7	59,9	119,9	253,8	*	41,7	191,9	222,4	*
160	89,7	179,9	192,5	67,2	137,4	225,5	*	39,1	183,6	222,0	*
184	87,7	161,1	168,7	70,9	140,3	201,7	*	37,6	166,4	200,3	*
Position	70 mm	35 mm	15 mm	130mm	75 mm	30 mm	0 mm	130mm	75 mm	30 mm	0 mm

* Connection to the thermocouple was lost.

Annex B
DESIGN MODELS

The Eurocode 3 prEN 1993-1-2: 2003 enables to predict the transfer of heat from the fire compartments to unprotected as well as protected steelwork. For an equivalent uniform temperature distribution in the cross-section, the increase of temperature $\Delta\theta_{a,t}$ in an unprotected steel member during a time interval Δt should be determined from clause 4.2.5.1 as

$$\Delta\theta_{a,t} = k_{sh} \frac{A_m / V}{c_a \rho_a} \dot{h}_{net,d} \Delta t \qquad \text{(B.1)}$$

where:

k_{sh} is correction factor for the shadow effect, which is used in case of nominal standard time temperature curves, the factor was not taken into account in prediction.

A_m / V is the section factor for unprotected steel members,

A_m is the surface area of the member per unit length,

V is the volume of the member per unit length,

c_a is the specific heat of steel,

$\dot{h}_{net,d}$ is the design value of the net heat flux per unit area,

Δt is the time interval, taken as 5 seconds

ρ_a is the unit mass of steel,

The value of $\dot{h}_{net,d}$ should be obtained from EN 1991-1-2 using $\varepsilon_f = 1,0$ and $\varepsilon_m = 0,7$, where ε_f, ε_m are as defined in EN 1991-1-2.

For a uniform temperature distribution in a cross-section, the temperature increase $\Delta\theta_{a,t}$ of an insulated steel member during a time interval Δt should be obtained from prEN 1993-1-2: 2003 par. 4.2.5.2 as

$$\Delta\theta_{a,t} = \frac{\lambda_p A_p / V}{d_p c_a \rho_a} \frac{(\theta_{g,t} - \theta_{a,t})}{(1 + \phi/3)} \Delta t - (e^{\phi/10} - 1) \Delta\theta_{g,t} \quad \text{(but } \Delta\theta_{a,t} \geq 0 \text{ if } \Delta\theta_{g,t} > 0) \qquad \text{(B.2)}$$

with:

$$\phi = \frac{c_p \rho_p}{c_a \rho_a} d_p A_p / V$$

where:

A_p / V is the section factor for steel members insulated by fire protection material;

A_p is the appropriate area of fire protection material per unit length of the member, which should generally be taken as the area of its inner surface, but for hollow encasement with a clearance around the steel member the same value as for hollow encasement without a clearance may be adopted:

V is the volume of the member per unit length,

c_a is the temperature dependant specific heat of steel,

c_p is the temperature independent specific heat of the fire protection material,

d_p is the thickness of the fire protection material,

Δt is the time interval taken as 30 seconds,

$\theta_{a,t}$ is the steel temperature at time t,

$\theta_{g,t}$ is the ambient gas temperature at time t,

$\Delta\theta_{g,t}$ is the increase of the ambient gas temperature during the time interval Δt,

λ_p is the thermal conductivity of the fire protection system;

ρ_a is the unit mass of steel,

ρ_p is the unit mass of the fire protection material.

For beam to column and beam to beam connections, where the beams are supporting any type of concrete floor, the temperature for the connection may be obtained from the temperature of the bottom flange at mid span. The connection temperature may be predicted, if the depth of the beam is less than 400 mm, see prEN 1993-1-2: 2003 Annex D 3.1, as

$$\theta_h = 0{,}88\ \theta_o\ (1 - 0{,}3\ h/D), \tag{B.3}$$

where

θ_a is the temperature at height h of the steel beam,

θ_o is the bottom flange temperature of the steel beam remote from the connection,

h is the height of the component being considered above the bottom of the beam,

D is the depth of the beam.

Annex C
DIFFERENTIAL METHOD FOR SLAB TEMPERATURE CALCULATION

Heating of the member depends on the heat transfer between the surrounding environment and the heat conduction within the member. This is expressed by Fourier heat transfer equation for nonsteady heat conduction inside the member

$$\frac{\partial}{\partial x}\left(\lambda_x \frac{\partial\theta}{\partial x}\right)+\frac{\partial}{\partial y}\left(\lambda_y \frac{\partial\theta}{\partial y}\right)+\frac{\partial}{\partial z}\left(\lambda_z \frac{\partial\theta}{\partial z}\right)+\overline{Q}=\rho\, c\, \frac{\partial\theta}{\partial t} \tag{C.1}$$

where

$\lambda_x, \lambda_y, \lambda_z,$ are thermal conductivities,

ρ is density,

c is specific heat capacity,

θ is temperature,

$\overline{Q}$ is internally generated heat.

In preliminary calculations of the slab temperatures the simplification into one-dimensional problem is possible

$$\frac{\partial}{\partial x}\left(\lambda_x \frac{\partial\theta}{\partial x}\right)=\rho\, c\, \frac{\partial\theta}{\partial t} \tag{C.2}$$

Boundary conditions are defined by time-temperature curve and by heat transfer, which is characterised by heat transfer coefficients - convective and radiative. Dominant at high temperatures is radiation component, which can be estimated as

$$\alpha_r = \frac{5{,}77\ \varepsilon_r}{\theta_g - \theta_k}\left[\frac{(\theta_g + 273)^4}{100^4} - \frac{(\theta_k + 273)^4}{100^4}\right] \qquad \text{(C.3)}$$

where

ε_r is resultant emissivity,
θ_g is gas temperature,
θ_k is member surface temperature.

Different heat transfer coefficients according to different authors are shown in Tab. C.1.

Tab. C.1 Heat transfer coefficients

Literature		α_r	α_c
(Karpaš and Zoufal, 1989)	exposed concrete surface	$\alpha_r = \frac{3{,}75}{\theta_g - \theta_k}\left[\frac{(\theta_g + 273)^4}{100^4} - \frac{(\theta_k + 273)^4}{100^4}\right]$	16,7
	not exposed concrete surface	$\alpha_r = \frac{4{,}64}{\theta_g - \theta_k}\left[\frac{(\theta_g + 273)^4}{100^4} - \frac{(\theta_k + 273)^4}{100^4}\right]$	11,4
(Pettersson et al, 1976)	exposed surface	$\alpha_r = \frac{5{,}77\varepsilon_r}{\theta_g - \theta_k}\cdot\left[\frac{(\theta_g + 273)^4}{100^4} - \frac{(\theta_k + 273)^4}{100^4}\right]$ $\varepsilon_r = \frac{1}{1/\varepsilon_m + 1/\varepsilon_f - 1}$	23
	not exposed surface	$0{,}033\,\theta_u$; where θ_u is temperature of non-exposed surface	8,7
(ENV 1991-1-2: 1994)	exposed surface	$\alpha_r = \frac{\Phi\ 5{,}67\ \varepsilon_r}{\theta_g - \theta_k}\left[\frac{(\theta_g + 273)^4}{100^4} - \frac{(\theta_k + 273)^4}{100^4}\right]$ $\Phi = 1{,}0;\ \varepsilon_m \,.\, \varepsilon_f = 0{,}7*0{,}8 = 0{,}56$	25
	not exposed surface	neglected	9
(ENV 1991-1-2: 2002)	exposed surface	$\alpha_r = \frac{\Phi\ 5{,}67\ \varepsilon_r}{\theta_g - \theta_k}\left[\frac{(\theta_g + 273)^4}{100^4} - \frac{(\theta_k + 273)^4}{100^4}\right]$ $\Phi = 1{,}0;\ \varepsilon_m \,.\, \varepsilon_f = 0{,}8*1{,}000 = 0{,}8$	35
	not exposed surface	9	

In table ε_f is the emissivity of flames and ε_m is the emissivity of the surface.

In differential method in one-dimensional heat transfer the Fourier equation (C.2) is simplified in the form

$$\frac{\Delta\theta}{\Delta t} = \frac{\lambda}{c\ \rho}\frac{\Delta^2\theta}{\Delta x^2} \qquad \text{(C.4)}$$

The slab is divided into layers. The layer thickness Δx cannot be too big, for $1000 < \rho < 2000$ the recommended maximum layer thickness is 20 mm. Temperatures are calculated in time intervals

$$\Delta t \le \frac{\Delta x^2}{2\,a} \text{ with } a = \frac{\lambda}{c\,\rho} \tag{C.5}$$

Temperature of the surface layer is calculated as

$$\theta_{1,t+1} = C_1.\ \theta_{N,t} + C_2.\ \theta_{1,t} + C_3.\ \theta_{2,t}\,, \tag{C.6}$$

where

$\theta_{N,t}$ is the surface temperature,
$\theta_{1,t}$ and $\theta_{2,t}$ are temperatures of inner layers,
C_1, C_2 and C_3 are coefficients as a function of material properties λ, c, ρ and heat transfer coefficient $\alpha = \alpha_r + \alpha_c$.

Temperature of the internal layer is calculated as

$$\theta_{m,t+1} = C_4.\ \theta_{m-1,t} + C_5.\ \theta_{m,t} + C_4.\ \theta_{m+1,t} \tag{C.7}$$

where

$\theta_{m,t}$ is the internal layer temperature,
C_4 and C_5 are coefficients as a function of material properties λ, c and ρ.

Influence of the moisture content is taken into account by the temperature increment, which expresses the amount of heat necessary to evaporation of water.

$$\Delta\theta_m = \frac{\overline{E}}{100} 2{,}26 \cdot 10^6 \frac{v}{100\,c}, \tag{C.8}$$

where

$\overline{E}$ is evaporating water in % (for members heated from one side = 40%),
$2{,}26 \cdot 10^6$ is the heat necessary for water evaporation,
v is the moisture content.

When the temperature of 100°C is reached, all other temperatures will be 100°C till the moment, when temperature increment is bigger than $\Delta\theta_m$. After this moment the calculations continue in normal way.